



# Application value of dual-energy computed tomography spectrum curve combined with clinical risk factors in predicting adherent perinephric fat

Guan Li<sup>1</sup>, Wei Huang<sup>1</sup>, Qinmei Xu<sup>1</sup>, Jie Dong<sup>2</sup>, Zhiqiang Cao<sup>3</sup>, Di Wang<sup>4</sup>, Mingyu Zou<sup>5</sup>, Guangming Lu<sup>1</sup>

<sup>1</sup>Department of Radiology, <sup>2</sup>Department of Urology, Jinling Hospital, Nanjing Medical University, Nanjing 210002, China; <sup>3</sup>Department of Urology, <sup>4</sup>Department of Pathology, <sup>5</sup>Department of Radiology, General Hospital of Northern Theater Command, Shenyang 110016, China.

Correspondence to: Guangming Lu. Department of Radiology, Jinling Hospital, Nanjing Medical University, Nanjing 210002, China.  
Email: cjr.luguangming@vip.163.com.

**Background:** Adherent perinephric fat (APF) is evaluated preoperatively with the Mayo adhesive probability (MAP) scoring system using conventional single form computed tomography (CT) images. An objective or quantitative indicator for predicting APF is urgently needed for clinical application.

**Methods:** Data obtained from 150 renal tumor patients with partial nephrectomy (PN) were used in the present study. Patients were divided into two groups based on the surgical results: an APF group (n=100) and a non-APF group (n=50). All patients had renal contrast-enhanced dual-energy CT (DECT) scan, and the data were brought into a post-processing workstation. Monoenergetic plus mode was adopted to analyze the spectrum curve of the region of interest (ROI). Logistic stepwise relapse investigation was utilized to analyze the related risk factors. The maximum Youden index was taken as the cut-off value. The sensitivity, specificity, accuracy, and 95% CI of the model were calculated.

**Results:** APF is related to patients' clinical characteristics of age, gender, BMI, smoking, tumor diameter, exophytic, and benign or malignant nature of the renal masses ( $P < 0.05$ ). The shape of the curve of ROI<sub>1</sub> in the APF group was different from that of the ROI<sub>4</sub> in the non-APF group, and the curve slope of K1 ( $-0.21 \pm 0.47$ ) was different from that of K4 ( $-1.30 \pm 0.14$ ) ( $P < 0.001$ ). Statistical analysis showed that the slope K was solely retained in the model index. The best cut-off point for the K value was  $-0.95$ . The AUC of the cut-off point was 0.97 (95% CI: 0.96–0.99).

**Conclusions:** The DECT spectrum curve performed well in predicting APF, and the curve slope K can be used as an objective quantitative indicator.

**Keywords:** Dual-energy computed tomography (DECT); spectrum curve; adherent perinephric fat (APF); partial nephrectomy (PN)

Submitted Feb 19, 2019. Accepted for publication Jun 26, 2019.

doi: 10.21037/qims.2019.06.22

View this article at: <http://dx.doi.org/10.21037/qims.2019.06.22>

## Introduction

Partial nephrectomy (PN) has become the gold standard treatment for small renal tumors (1). As indicated by the guidelines of the American Urological Association (AUA), PN is the primary choice for patients with T1aN0M0 stage renal carcinoma (2). Precise preoperative assessment of

surgical difficulty and risk factor prediction is the key to perform PN successfully. Kutikov *et al.* (3) first proposed a standardized scoring system for renal tumor characteristics in 2009, namely the R.E.N.A.L. nephrometry score. However, this scoring framework surveyed the specialized attainability of PN only based on the renal tumor characteristics and did not take the impact of the surrounding kidney conditions

into account. At the point when adherent perinephric fat (APF) presents, it can prompt the increased difficulty of surgical stripping, prolong operation time, and increase bleeding and tearing, even from PN conversion to radical nephrectomy (RN). Davidiuk *et al.* (4) first proposed the impact of APF on PN in 2014 and established a computed tomography (CT) imaged-based Mayo adhesive probability (MAP) score to predict the possibility of APF before surgery.

APF, also known as perinephric sticky fat (PSF), can be defined as a linear area of soft tissue attenuation in the perinephric space (5,6). On CT images, it tends to be viewed as perinephric fat stranding. As per the circumstance of the perinephric fat stranding, MAP score divides perinephric fat stranding into three grades: 0 points (no stranding), 2 points (type 1, some image-dense stranding but no thick bars of inflammation), or 3 points (type 2, severe stranding and having thick bars of inflammation) (4). There is a highly subjective effect in evaluating the perinephric fat stranding grades. This outcome specifically influences the final results of the MAP score and affects the accuracy of preoperative risk assessment.

DECT provides more image information than traditional single-energy CT, and DECT post-processing software provides more techniques for assessing APF. Since DECT has two distinctive tube voltages for X-ray emission, the X-ray attenuation data at high and low energy can be acquired, and the chemical composition, content, and physical properties can be analyzed (7,8). The DECT spectrum curve is based on the attenuation degree of X-ray absorption of substances with different characteristics (9). The present study is based on another assessment framework for foreseeing APF by combining the DECT spectrum curve with pertinent clinical indicators to anticipate APF more accurately.

## Methods

### *Patient population*

A total of 150 patients with renal tumors had PN in Jinling Hospital, Nanjing Medical University between August 2017 to November 2018. Of these patients, 89 were males, and 61 were females, with an age range of 25 to 83, and a mean age of  $52.32 \pm 11.93$  years. According to the surgical records (4,5), 150 patients were divided into two groups according to the presence of APF: an APF group ( $n=100$ ) and a non-APF group ( $n=50$ ). An institutional review board endorsed this retrospective study, and informed consent was waived.

The inclusion criteria were as follows: (I) initially diagnosed as T1 stage renal tumors by ultrasonography, CT, and MRI; (II) with renal enhanced DECT examination before operation; (III) PN performed by the same surgeon; (IV) surgical records for diagnosis of APF or non-APF. The exclusion criteria were as follows: (I) contrast agent allergy and other contraindications; and (II) secondary surgery due to renal tumor recurrence. The general clinical data and tumor characteristics of the patients were collected.

### *DECT data acquisition*

Renal three-phase dynamic contrast-enhanced DECT scan was performed by dual-energy CT (SOMATOM Definition Flash, Siemens Healthcare, Forchheim, Germany). The scanning parameters were as follows: tube voltage and tube current, tube A 100 kVp, 149 eff.mAs and tube B Sn 140 kVp, 117 eff.mAs; gantry rotation time, 0.5 s; detector configuration, 64 mm $\times$ 0.6 mm; pitch, 1.2; slice thickness, 5 mm; and FOV, 260 mm. Automatic current modulation (CareDose4D; Siemens Healthcare) was used for all scans. The contrast agent iohexol (Omnipaque 350, GE Healthcare, USA) was injected into the anterior cubital vein with a dual-cylinder high-pressure syringe (Urich, Medical, USA) at a rate of 4 mL/s and a dose of 1.5 mL/kg, with a total volume of about 60–80 mL. The region of interest (ROI) was placed at the branch level of the abdominal aorta and renal artery by using Bolus Tracking software (Bolus Tracking). When the threshold reached 100 HU, renal arterial phase CT scanning was performed after a delay of 7 s, followed by a delay of 40 s and 5 min for the renal venous phase and delayed phase scanning, respectively.

### *Spectrum curve analysis*

All renal venous phase CT DICOM data were transmitted to the DECT post-processing workstation (Syngo Version VB10, Siemens Healthcare, Forchheim, Germany). The ROI measurements were completed in monoenergetic plus mode. To assure the appropriate placement of ROIs, measurements were performed in consensus between two doctors, a radiologist and a urologist, who had 10 and 20 years of work experience respectively. The mean values and standard deviations were recorded. The selection criteria of ROIs were as follows: (I) ROI<sub>1</sub>, (APF group) the most obvious area of peritumoral APF (avoiding the tumors and regenerating blood vessels); (II) ROI<sub>2</sub>, (APF group) perirenal fat in corresponding area on the healthy side; (III)

ROI<sub>3</sub>, (APF group) lateral abdominal subcutaneous fat; (IV) ROI<sub>4</sub>, (non-APF group) perirenal fat around the tumor; (V) ROI<sub>5</sub>, (non-APF group) perirenal fat in corresponding area on the healthy side; and (VI) ROI<sub>6</sub>, (non-APF group) lateral abdominal subcutaneous fat. The consistencies of ROI measurement size, shape, location, and composition were ensured. The area of each ROI was 0.5 cm<sup>2</sup>. The slope of the ROI curve was calculated according to the slope (K) formula of the spectrum curve ( $K = |HU_{40\text{ keV}} - HU_{110\text{ keV}}| \div 110\text{ keV} - 40\text{ keV}$ ).

### Pathological analysis

Pathological analysis of tumor and perirenal adipose tissue was done for the 150 patients with surgical resection. The specimens were fixed with formalin, then dehydrated, embedded with paraffin, and followed by section cutting with the thickness of 4 mm, and finally stained with conventional H&E staining. Fluorescence microscope biomicroscopy (Olympus BX43) was used to observe the slices. The field of view was selected as “×40, ×100”.

### Statistical analysis

Statistical data analysis was performed using SPSS 25.0 software. Measurement data were expressed as mean ± standard deviation (SD). Student's *t*-test was used for comparison between the two groups. Numeration data were expressed by the number of cases and the percentage [n (%)]. Chi-square test and Fisher's exact test were used to compare categorical data. Univariate and multivariate logistic regression analyses were performed to evaluate preoperative predictive factors of APF. A multivariable logistic regression model was developed using a forward selection approach, with a focus on improvement in the area under the receiver operating characteristic curve (AUC). Odds ratio (OR) and 95% CI were given. The maximum Youden index was used as the best cut-off point. Sensitivity, specificity, and accuracy were calculated to assess the efficiency of the model. The area under the curve (AUC) of the MAP and Model were calculated and compared by Delong's test. The sensitivity, specificity, and accuracy of MAP and Model were analyzed by the McNemar test. A *P*<0.05 was considered statistically significant.

## Results

Table 1 summarizes the demographic characteristics of the cohort. Patients with APF were significantly older

(55.42±10.95 *vs.* 46.12±11.44, for the non-APF patients, *P*<0.001) and had a higher BMI (30.64±4.14 *vs.* 26.02±4.66, for non-APF patients, *P*<0.001) than the non-APF patients. Furthermore, the proportion of males and smokers were higher in the APF group compared with the non-APF group (73.0% *vs.* 32.0%, 66.0% *vs.* 34.0%, *P*<0.001).

Table 2 shows an evaluation of the correlation between tumor characteristics and APF. The largest proportion of renal tumor diameter had a diameter of 4 to 7 cm (48.0%) in the APF group, and less than 4 cm (64.0%) in the non-APF group. Renal tumors with more than 50% exogenous are malignant, and those in the APF group were significantly higher than the non-APF group (63.0% *vs.* 26.0%, *P*<0.001). The proportion of malignant tumors in the APF group (94.0%) was also higher than that in the non-APF group (58.0%, *P*<0.001).

The ROI measurements are different in the curve shape and slope (K) of ROI<sub>1</sub>, ROI<sub>2</sub>, and ROI<sub>3</sub> in the APF group (all *P*<0.001), indicating that these adipose tissues might have different ingredients or contents. The curve shape and slope (K) of ROI<sub>1</sub> are significantly different from ROI<sub>4</sub> (*P*<0.001), suggesting that the spectrum curve could effectively distinguish APF from non-APF. The curve shape and slope (K) of ROI<sub>2</sub> are significantly different from ROI<sub>5</sub> (*P*<0.001), while ROI<sub>4</sub> and ROI<sub>5</sub> are not (*P*=0.496). These data indicate that APF occurred in both perinephric areas. We believe that systemic APF and its extent can be aggravated by the local factors of renal tumors. The curve shape and slope (K) of ROI<sub>3</sub> are not significantly different from ROI<sub>6</sub> (*P*=0.348), and ROI<sub>4</sub> and ROI<sub>5</sub> differed from ROI<sub>6</sub> (all *P*<0.001). This observation confirms that perinephric fat was different from abdominal subcutaneous fat (Table 3 and Figure 1,2).

The slope (K) as the only indicator with statistical differences (*P*<0.05) in the results of the univariate analysis were included in the final logistic model [OR =1.594 (95% CI: 1.380–1.841, *P*<0.001)]. The slope (K) can be effectively and accurately predict APF. The best cut-off point of K value was -0.95 (K <-0.95 was non-APF, K ≥-0.95 was APF). All patients were measured by MAP score. The results showed that the model had higher AUC, specificity, sensitivity, and accuracy than the MAP score (*P*<0.01) (Table 4).

Figure 3 displays the gross samples of APF and non-APF. While no obvious differences are discernible by the naked eye, microscopic changes in neovascularization, hyperemia with a small amount of lymphocyte infiltration, and different degrees of fibrous tissues in the APF group were observed. Normal adipocytes were found only in the non-APF group.

**Table 1** Comparison of demographic characteristics between the APF group and non-APF group

Variable	APF (n=100)	non-APF (n=50)	OR (95% CI)	P
Age, mean $\pm$ SD (years)	55.42 $\pm$ 10.95	46.12 $\pm$ 11.44	1.075 (1.040, 1.112)	<0.001
Gender, n (%)				<0.001
Female	27 (27.0)	34 (68.0)	Reference	
Male	73 (73.0)	16 (32.0)	5.745 (2.741, 12.045)	
BMI, mean $\pm$ SD (kg/m <sup>2</sup> )	30.64 $\pm$ 4.14	26.02 $\pm$ 4.66	1.259 (1.150, 1.379)	<0.001
Hypertension, n (%)				0.729
Yes	49 (49.0)	23 (46.0)	1.128 (0.571, 2.227)	
No	51 (51.0)	27 (54.0)	Reference	
Diabetes, n (%)				0.458
Yes	34 (34.0)	14 (28.0)	1.325 (0.630, 2.785)	
No	66 (66.0)	36 (72.0)	Reference	
Smoking, n (%)				<0.001
Yes	66 (66.0)	17 (34.0)	3.768 (1.840, 7.715)	
No	34 (34.0)	33 (66.0)	Reference	
Alcoholism, n (%)				0.386
Yes	22 (22.0)	8 (16.0)	1.481 (0.607, 3.613)	
No	78 (78.0)	42 (84.0)	Reference	
Preoperative eGFR <60 mL/min, n (%)				0.087
Yes	19 (19.0)	4 (8.0)	2.698 (0.865, 8.412)	
No	81 (81.0)	46 (92.0)	Reference	

APF, adherent perinephric fat; eGFR, estimated glomerular filtration rate.

## Discussion

APF is a vital factor that cannot be ignored in PN for renal tumors. Preoperative accurate prediction of APF is useful for devising a careful surgical plan, assessing surgical risk, and reducing surgical complications. In the present study, which compared the demographic and tumor characteristics between the APF group and the non-APF group, the statistical results showed that age, gender, BMI, smoking, tumor diameter, and malignancy were closely related to the presence and severity of APF (all  $P < 0.05$ ). Although these indicators were not applied in the final model, they could still be used as risk factors to predict APF. On this basis, combined with the spectrum curve of DECT, the changes of perineal fat can be observed intuitively. More accurate and objective prediction of APF could be made using the spectrum curve shape and the best cut-off point of the curve slope (K).

APF has a certain correlation with BMI. Lee *et al.* consider APF to be related to metabolic syndrome (MetS) and can be evaluated within the range of disorders, including glucose intolerance, dyslipidemia, and hypertension (10). Higher BMI and being overweight can lead to MetS (11,12). The present study identified smoking to be associated with a high risk of APF in the study patients, although it is not conclusive whether smoking is a risk factor of APF in the literature (4,5). Davidiuk *et al.* reported a positive correlation (4), but Bylund *et al.* study did not support these findings (5). The limited number of only 29 enrolled cases may explain Bylund's results. Cheng *et al.* (13) proposed that cigarette smoking was associated with MetS, and smokers had a higher BMI compared to non-smokers. The proportion of smokers was higher in the APF group compared with the non-APF group in our study.

Many factors such as inflammatory microenvironment,

**Table 2** Comparison of tumor characteristics between the APF group and non-APF group

Tumor characteristics	APF (n=100)	non-APF (n=50)	OR (95% CI)	P
Tumor diameter, n (%) (cm)				0.020
≤4	40 (40.0)	32 (64.0)	Reference	
4–7	48 (48.0)	13 (26.0)	2.954 (1.369, 6.374)	
>7	12 (12.0)	5 (10.0)	1.920 (0.613, 6.016)	
Tumor location, n (%)				0.623
Upper	33 (33.0)	18 (36.0)	Reference	
Middle	40 (40.0)	16 (32.0)	1.364 (0.603, 3.084)	
Lower	27 (27.0)	16 (32.0)	0.920 (0.396, 2.140)	
Tumor exophytic, n (%)				<0.001
>50%	63 (63.0)	13 (26.0)	4.846 (2.287, 10.270)	
<50%	37 (37.0)	37 (74.0)	Reference	
Benign or malignant, n (%)				<0.001
Malignant	94 (94.0)	29 (58.0)	11.345 (4.181, 30.784)	
Benign	6 (6.0)	21 (42.0)	Reference	

APF, adherent perinephric fat.

**Table 3** Statistical description of different ROI slopes (K) in the two Groups

Location	Group		P
	APF	non-APF	
ROI <sub>1</sub> (ROI <sub>4</sub> )	-0.21±0.47	-1.30±0.14	<0.001
ROI <sub>2</sub> (ROI <sub>5</sub> )	-0.99±0.20	-1.28±0.13	<0.001
ROI <sub>3</sub> (ROI <sub>6</sub> )	-1.49±0.17	-1.52±0.19	0.348

ROI, region of interest; APF, adherent perinephric fat.

MetS, autoimmune response, and idiopathic fibrosis had been reported to relate to APF, however the pathological mechanism of APF was still unclear (14-16). Activation of a chronic inflammation system can cause endothelial cells to secrete a variety of cytokines, chemokines, and plasminogen activator inhibitor type 1 (PAI-1), thereby reducing the fibrinolytic activity and leading to fibrous adhesion between perirenal fat and the renal capsule (17,18). In addition, serotonin [5-hydroxytryptamine (5-HT)], considered as fibrosis-related growth factor which is highly expressed in renal cell carcinoma contributes to APF (19,20). These paracrine mechanisms may partially explain why the probability of APF in benign renal tumors was lower than that in malignant tumors in our study.

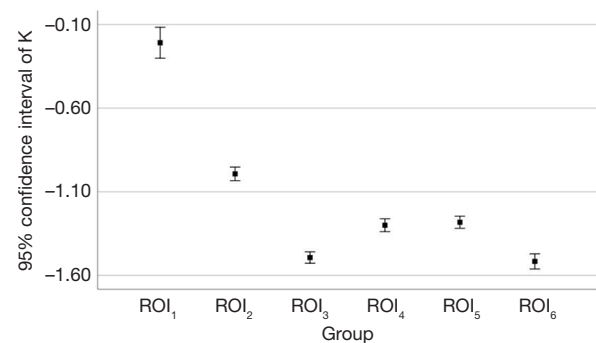


**Figure 1** Mean and 95% CI of the six ROIs slope K. ROI, region of interest.

In this examination, ROI was measured in the renal venous phase because the kidney and perinephric tissues showed more clearly in this phase. The DECT spectrum curve is based on the different substances having corresponding X-ray linear attenuation coefficients. When the high and low tube instantaneously switch, the X-ray decay degree of the transmitter substance is different, and the spectrum curves of different substances and different energies can be acquired (21,22). Although the normal spectrum CT curve ranges from 40–190 keV, a 40–110 keV interval was chosen in the present study since the shape of

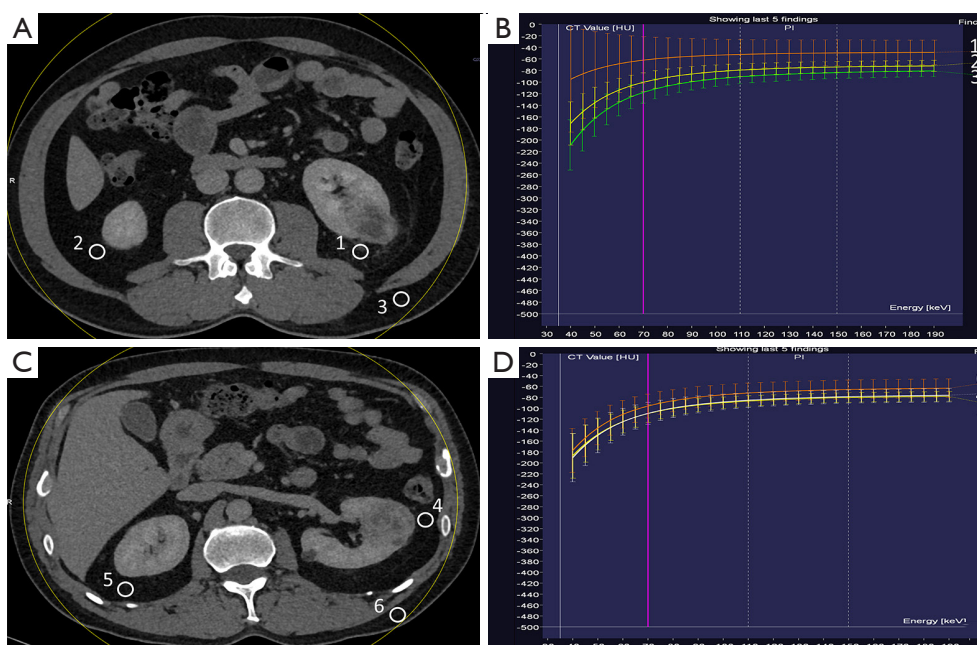


**Figure 2** Measurement of ROIs in the APF and non-APF groups, and the results of the spectrum curve under monoenergetic plus mode. Panels A~D show the ROI selection and corresponding spectrum curve shape in the APF group and non-APF group, respectively. ROI, region of interest; APF, adherent perinephric fat.

**Table 4** Diagnostic efficiency of MAP and model

Pattern	AUC (95% CI)	Sensitivity (95% CI)	Specificity (95% CI)	Accuracy (95% CI)	P
MAP	0.85 (0.78–0.92)	0.84 (0.85–0.96)	0.86 (0.74–0.93)	0.85 (0.78–0.90)	<0.01
Model	0.97 (0.96–0.99)	0.97 (0.90–0.99)	0.95 (0.89–0.98)	0.96 (0.92–0.98)	

MAP, Mayo adhesive probability; ROI, region of interest; APF, adherent perinephric fat.

the spectrum curve of ROI was more characteristic, and the slope (K) was more specific within this range.

There are a few limitations to our investigation. The sample size of this study is relatively small, and the conclusions of this research need to be further studied in a larger data set. Furthermore, our investigation lacks the spectrum curve analysis of APF in different pathological types of renal tumors. Moreover, the results have not been compared to other kinds of DECT from different manufacturers. Finally, the existence of APF can be confirmed by the surgeon's feedback, but a standard for

determining APF degree is still lacking. Given this, the use of the DECT spectrum curve in the prediction of different degrees of APF requires further investigation.

## Conclusions

DECT spectrum curve analysis can be effectively used to predict the presence of APF, and the slope (K) of the spectrum curve might be a potential target quantitative marker. Furthermore, combined relevant clinical risk factors are expected to become a new method for predicting APF.

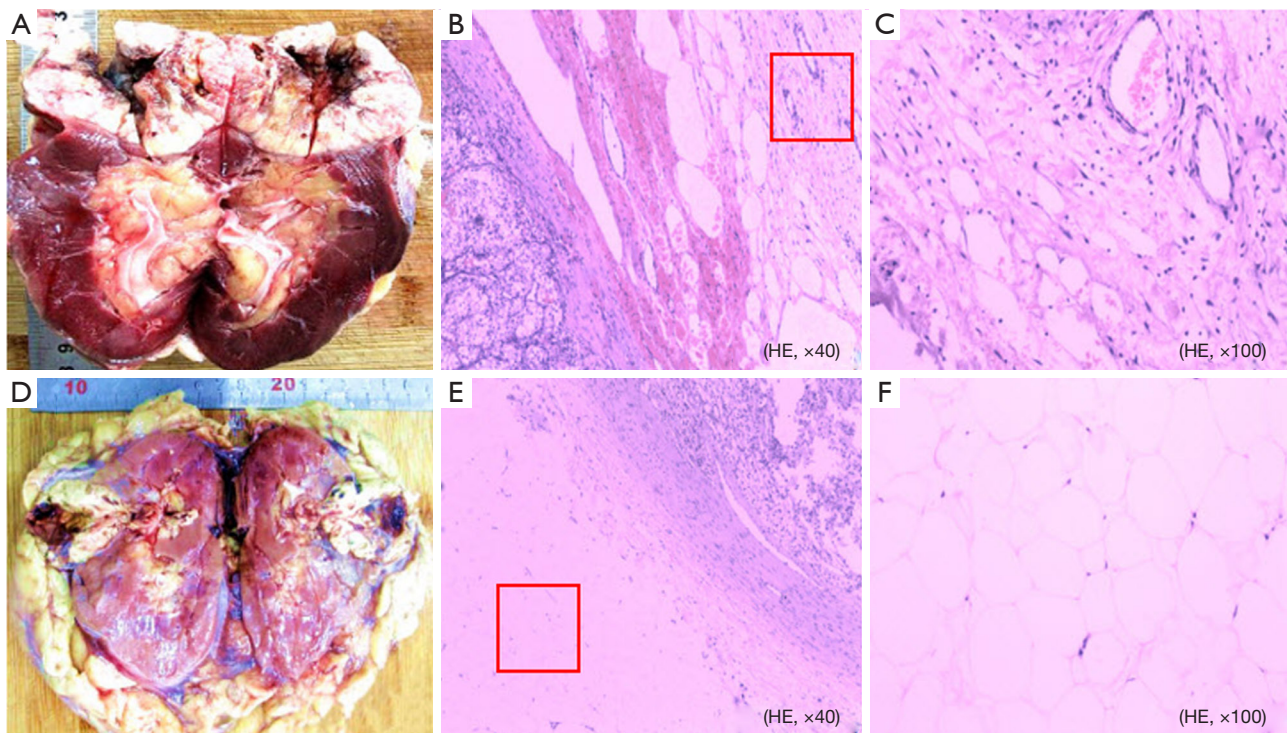


**Figure 3** Gross and microscopic photographs of APF and non-APF. Panels A and D show gross appearance in the APF and non-APF. Panels B and C, and Panels E and F are photomicrographs (HE,  $\times 40$ ,  $\times 100$ ) of APF and non-APF respectively. Panels C and F are the areas corresponding to the red box in Panel B and E, respectively. APF, adherent perinephric fat.

### Acknowledgments

**Funding:** This study was supported by the National Clinical Key Specialist Military Construction Project of China and the Clinical Medical Imaging Center Project of Jiangsu Province, China (grant YXZZA2016007).

### Footnote

**Conflicts of Interest:** The authors have no conflicts of interest to declare.

**Ethical Statement:** Our institutional review board approved this retrospective study, and informed consent was waived since this was a retrospective study.

### References

1. Lee SY, Choi JD, Seo SI. Current status of partial nephrectomy for renal mass. *Korean J Urol* 2011;52:301-9.
2. Sui G, Luo Q, Du J, Teng D, Wang H. Clinical application of ultrasound-guided percutaneous microwave ablation in the treatment of T1aN0M0 stage renal carcinoma. *J Med Ultrason* (2001) 2019;46:217-22.
3. Kutikov A, Uzzo RG. The R.E.N.A.L. nephrometry score: a comprehensive standardized system for quantitating renal tumor size, location and depth. *J Urol* 2009;182:844-53.
4. Davidiuk AJ, Parker AS, Thomas CS, Leibovich BC, Castle EP, Heckman MG, Custer K, Thiel DD. Mayo adhesive probability score: an accurate imaged-based scoring system to predict adherent perinephric fat in partial nephrectomy. *Eur Urol* 2014;66:1165-71.
5. Bylund JR, Qiong H, Crispin PL, Venkatesh R, Strup SE. Association of clinical and radiographic features with perinephric "sticky" fat. *J Endourol* 2013;27:370-3.
6. Kawamura N, Saito K, Inoue M, Ito M, Kijima T, Yoshida S, Yokoyama M, Ishioka J, Matsuoka Y, Kihara K, Fujii Y. Adherent Perinephric Fat in Asian Patients: Predictors and Impact on Perioperative Outcomes of Partial Nephrectomy. *Urol Int* 2018;101:437-42.
7. Shi JW, Dai HZ, Shen L, Xu DF. Dual-energy CT:

- clinical application in differentiating an adrenal adenoma from a metastasis. *Acta Radiol* 2014;55:505-12.
8. Goo HW, Goo JM. Dual-Energy CT: New Horizon in Medical Imaging. *Korean J Radiol* 2017;18:555-69.
  9. Aran S, Daftari Besheli L, Karcaaltincaba M, Gupta R, Flores EJ, Abujudeh HH. Applications of dual-energy CT in emergency radiology. *AJR Am J Roentgenol* 2014;202:W314-24.
  10. Lee SM, Robertson I, Stonier T, Simson N, Amer T, Aboumarzouk OM. Contemporary outcomes and prediction of adherent perinephric fat at partial nephrectomy: a systematic review. *Scand J Urol* 2017;51:429-34.
  11. Batsis JA, Mackenzie TA, Bartels SJ, Sahakyan KR, Somers VK, Lopez-Jimenez F. Diagnostic accuracy of body mass index to identify obesity in older adults: NHANES 1999-2004. *Int J Obes (Lond)* 2016;40:761-7.
  12. Egert S, Baxheinrich A, Lee-Barkey YH, Tschoepe D, Stehle P, Stratmann B, Wahrburg U. Effects of a hypoenergetic diet rich in  $\alpha$ -linolenic acid on fatty acid composition of serum phospholipids in overweight and obese patients with metabolic syndrome. *Nutrition* 2018;49:74-80.
  13. Cheng E, Burrows R, Correa P, Güichapani CG, Blanco E, Gahagan S. Light smoking is associated with metabolic syndrome risk factors in Chilean young adults. *Acta Diabetol* 2019;56:473-9.
  14. Khene ZE, Peyronnet B, Mathieu R, Fardoun T, Verhoest G, Bensalah K. Analysis of the impact of adherent perirenal fat on peri-operative outcomes of robotic partial nephrectomy. *World J Urol* 2015;33:1801-6.
  15. Timar O, Sestier F, Levy E. Metabolic syndrome X: a review. *Can J Cardiol* 2000;16:779-89.
  16. Macleod LC, Hsi RS, Gore JL, Wright JL, Harper JD. Perinephric fat thickness is an independent predictor of operative complexity during robot-assisted partial nephrectomy. *J Endourol* 2014;28:587-91.
  17. Kosaka H, Yoshimoto T, Yoshimoto T, Fujimoto J, Nakanishi K.. Interferon-gamma is a therapeutic target molecule for prevention of postoperative adhesion formation. *Nat Med* 2008;14:437-41.
  18. Trayhurn P, Wood IS. Adipokines: inflammation and the pleiotropic role of white adipose tissue. *Br J Nutr* 2004;92:347-55.
  19. Jungwirth N, Haeberle L, Schrott KM, Wullich B, Krause FS. Serotonin used as prognostic marker of urological tumors. *World J Urol*. 2008;26:499-504.
  20. Chen L, Chen G, Guo Y, Liu L, Xiao L, Fan W, Shi B, Qian Y. Ketanserin, a serotonin 2A receptor antagonist, alleviates ischemia-related biliary fibrosis following donation after cardiac death liver transplantation in rats. *Liver Transpl* 2014; 20:1317-26.
  21. Wisenbaugh ES, Paden RG, Silva AC, Humphreys MR. Dual-energy vs conventional computed tomography in determining stone composition. *Urology* 2014; 83:1243-7.
  22. Ha W, Sidky EY, Barber RF, Schmidt TG, Pan X. Estimating the spectrum in computed tomography via Kullback-Leibler divergence constrained optimization. *Med Phys* 2019;46:81-92.

**Cite this article as:** Li G, Huang W, Xu Q, Dong J, Cao Z, Wang D, Zou M, Lu G. Application value of dual-energy computed tomography spectrum curve combined with clinical risk factors in predicting adherent perinephric fat. *Quant Imaging Med Surg* 2019;9(8):1421-1428. doi: 10.21037/qims.2019.06.22